AD-A207 583 HYPERSONIC PREDICTION COMPARISONS WITH EXPERIMENTAL DATA FOR A CONE-CYLINDER AT MACH 686(U) AIR FORCE ARMAMENT LAB EGLIN AFB FL M C HUGHSON ET AL. MAR 89 1/1

UNCLASSIFIED AFATL-TP-89-04 F/G 20/4 NL

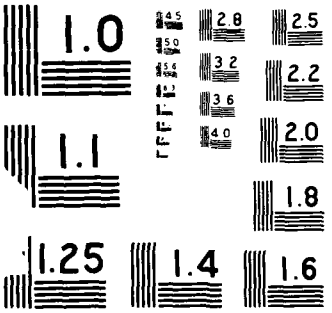
1.0
1.1
1.25
1.4
1.6
1.8
2.0
2.2
2.5
2.8
3.2
3.6
4.0
4.5
5.0

AIAA '89

(4)

AIAA-89-0524

Hypersonic Prediction Comparisons with Experimental Data for a Cone-Cylinder at Mach 6.86

M.C. Hughson and C.J. Cottrell, U.S. Air Force Armament Laboratory, Eglin AFB, FL

27th Aerospace Sciences Meeting
January 9–12, 1989/Reno, Nevada

REPORT DOCUMENTATION PAGE

Form Approved
OMB No. 0704-0188

1a. REPORT SECURITY CLASSIFICATION UNCLASSIFIED	1b. RESTRICTIVE MARKINGS
2a. SECURITY CLASSIFICATION AUTHORITY	3. DISTRIBUTION/AVAILABILITY OF REPORT Approved for public release; distribution unlimited.
2b. DECLASSIFICATION/DOWNGRADING SCHEDULE	
4. PERFORMING ORGANIZATION REPORT NUMBER(S)	5. MONITORING ORGANIZATION REPORT NUMBER(S) AFATL-TP-89-04
6a. NAME OF PERFORMING ORGANIZATION Aerodynamics Branch Aeromechanics Division 6b. OFFICE SYMBOL (If applicable) AFATL/FXA	7a. NAME OF MONITORING ORGANIZATION Aeromechanics Division Aerodynamics Branch
6c. ADDRESS (City, State, and ZIP Code) Air Force Armament Laboratory Eglin Air Force Base, FL 32542-5434	7b. ADDRESS (City, State, and ZIP Code) Air Force Armament Laboratory Eglin Air Force Base, FL 32542-5434
8a. NAME OF FUNDING/SPONSORING ORGANIZATION Aeromechanics Division 8b. OFFICE SYMBOL (If applicable) FXA	9. PROCUREMENT INSTRUMENT IDENTIFICATION NUMBER In-house
8c. ADDRESS (City, State, and ZIP Code) Eglin Air Force Base, FL 32542-5434	10. SOURCE OF FUNDING NUMBERS PROGRAM ELEMENT NO. 62602F; PROJECT NO. 2567; TASK NO 03; WORK UNIT ACCESSION NO. 08
11. TITLE (Include Security Classification) Hypersonic Prediction Comparisons with Experimental Data for a Cone-Cylinder at Mach 6.86	
12. PERSONAL AUTHOR(S) Hughson, Montgomery C. and Cottrell, Charles J.	
13a. TYPE OF REPORT Final 13b. TIME COVERED FROM Oct 88 TO Jan 89 14. DATE OF REPORT (Year, Month, Day) March 1989 15 PAGE COUNT 10	
16. SUPPLEMENTARY NOTATION This TP was not edited nor edited by AFATL/DOIR.	

17. COSATI CODES			18. SUBJECT TERMS (Continue on reverse if necessary and identify by block number)
FIELD	GROUP	SUB-GROUP	Experimental Aerodynamics, Hypersonic, Aerodynamics, Cone-Cylinder
20	04		

19. ABSTRACT (Continue on reverse if necessary and identify by block number)

Comparisons of computed flowfield predictions to experimental data for a cone-cylinder configuration at Mach 6.86 and angles of attack of 0, 6.7, 14, and 20 degrees are presented. The two inviscid computer codes used were EAGLE and ZEUS, which represent a time-iterative and a space-marching approach, respectively. Specific comparisons were made between the predicted and the experimental pressure distributions along the body at various circumferential locations, as well as aerodynamic characteristics of normal force coefficient and the location of the center of pressure. The inviscid calculations compare well with experimental data where viscous effects are minimal.

20. DISTRIBUTION/AVAILABILITY OF ABSTRACT ☐ UNCLASSIFIED/UNLIMITED ☒ SAME AS RPT. ☐ DTIC USERS	21. ABSTRACT SECURITY CLASSIFICATION UNCLASSIFIED
22a. NAME OF RESPONSIBLE INDIVIDUAL MONTGOMERY C. HUGHSON, 1Lt, USAF	22b TELEPHONE (Include Area Code) 904-882-3124 22c. OFFICE SYMBOL AFATL/FXA

DD Form 1473, JUN 86 *Previous editions are obsolete.*

HYPERSONIC PREDICTION COMPARISONS WITH EXPERIMENTAL DATA FOR A CONE-CYLINDER AT MACH 6.86

MONTGOMERY C. HUGHSON* and CHARLES J. COTTRELL**
Aeromechanics Division
Air Force Armament Laboratory
Eglin AFB FL 32542-5434

Abstract

Comparisons of computed flowfield predictions to experimental data for a cone-cylinder configuration at Mach 6.86 and angles of attack of 0, 6.7, and 14 degrees are presented. The two inviscid computer codes used were EAGLE and ZEUS, which represent a time-iterative, shock capturing approach, and a space-marching, shock fitting approach, respectively. Specific comparisons were made between the computed and the experimental surface pressure distributions along the body at various circumferential locations and around the body at axial locations on the conical nose and the cylindrical afterbody. Comparisons of the aerodynamic characteristics of normal force coefficient and the location of the center-of-pressure were also made. The inviscid calculations compare well with experimental data where viscous effects are minimal.

Introduction

The renewed interest in sustained hypersonic flight, coupled with the lack of ground-based test facilities in this flight regime, has focused attention on computational fluid dynamics (CFD) codes for hypersonic aerodynamic studies. Although inviscid codes obviously cannot address aerothermodynamic problems, the design engineer can use these codes for quick and efficient studies of aerodynamic characteristics. The purpose of this paper is to compare the hypersonic flowfield predictions of the EAGLE code to the ZEUS code and to experimental data for a cone-cylinder configuration at Mach 6.86 and angles-of-attack of 0, 6.7, and 14 degrees. EAGLE was developed for application in the high subsonic and transonic regimes. Confidence in its ability in the supersonic and hypersonic regimes will expand its usefulness as a design tool. The ZEUS code was selected for comparison because its validity in high Mach ranges is well documented.

In the next section a description of the configuration and the experimental data will be presented. The following section will give a brief discussion of each of the codes used, followed by a section presenting results of their usage. The last section will discuss conclusions.

Configuration and Experimental Data

The cone-cylinder configuration is shown in Figure 1. The conical nose had a half-angle of 10 degrees, and the cylindrical afterbody was 4 diameters long. The cone-cylinder was tested in the Langley 11-inch hypersonic tunnel, which achieved uniform flow for model testing at Mach 6.86 in a 5-inch square test section. The Reynold's number was 290,000 based on maximum diameter. A detailed description of the hypersonic tunnel can be found in References 1 and 2.

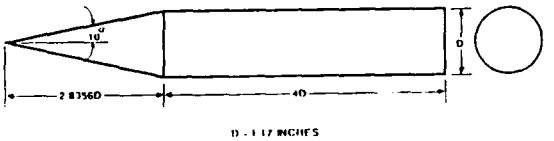

D = 1.17 INCHES

Figure 1. Cone-cylinder configuration.

The model was designed with a length of 8 inches in order to retain the model completely within the uniform flow region of the test section during the high angle-of-attack cases. The model was equipped with ten pressure orifices installed along the generatrix of the body, five on the conical nose, four on the cylindrical afterbody, and one on the base. The model was machined from steel and had a polished surface.

The pressure distribution over the model was obtained at circumferential positions corresponding to 0, 30, 60, 90, 120, 150, and 180 degrees for the 6.7 and 14 degree angle-of-attack cases, and only at the 0 circumferential position for the 0 angle-of-attack case. Force and moment measurements for the cone-cylinder model were obtained at intervals of about 3 or 4 degrees throughout the angle-of-attack range. A thorough description of the experiment can be found in Reference 3.

*1Lt, USAF, Computational Fluid Dynamics Section, Member AIAA
**Chief, Plans & Programs Branch Senior Member AIAA

Computer Codes

EAGLE

Program EAGLE (Eglin Arbitrary Geometry Implicit Euler) is a multiblock grid generation and steady-state flow solver system. This system combines a boundary conforming surface generation scheme, a composite block structure grid generation scheme, and a multiblock, implicit Euler flow solver algorithm. The three codes are intended to be used sequentially from the definition of the configuration under study to the flow solution about the configuration. Full documentation on each code's usage can be found in References 4-7. Program EAGLE has been used as a design aid in the analysis of both freestream and interference aerodynamic characteristics of single and multiple arbitrarily shaped bodies, finned and unfinned, in the high subsonic, and transonic Mach ranges.[8-12]

The computational grid built for the cone-cylinder configuration consisted of 2 similar three-dimensional blocks. Each block covered half the cone-cylinder configuration and was dimensioned at 75 x 25 x 37. That is, 75 lines along the body, 25 lines between the body surface and the outer boundary, and 37 lines circumferentially about the body. A cross-section of the grid is shown in Figure 2. NACA TR 1135 tables[13] were used to calculate the shock wave location from the body, and doubling that distance was used to determine the distance to the outer boundary of the grid. To obtain as smooth a grid as possible, the elliptic grid generator was employed for 100 iterations.

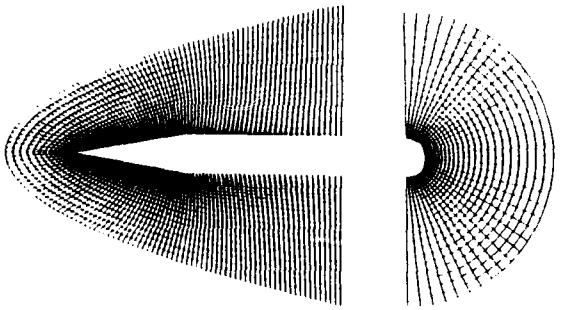

Side View End View

Figure 2. EAGLE code grid - 75 x 25 x 37 each half.

An Euler solver was used to predict the pressure distributions and force and moment calculations for the cone-cylinder configuration. The solver uses an implicit, two-pass upwind scheme, and is second order accurate in space. It uses the flux-difference splitting scheme of Roe and is stable for a wide range of Courant numbers for steady-state computations. All cases here were run with a Courant number of 4. The Euler equations are written in strong conservation law form in order to capture discontinuities in the flow, such as shocks. A finite volume formulation is used in order to achieve total flexibility with regard to geometry. Local time-stepping is used to accelerate convergence for steady-state problems. Characteristic variable boundary conditions are used by the solver on far field boundaries and at the body surface. As noted earlier, the outer boundary was placed far enough from the body to include all shocks within the solution domain, so freestream flow conditions were imposed at the outer grid surface, and extrapolation was used at the outflow plane.

The Euler code was run for 1,500 iterations, which coincidentally corresponded to a reduction of the L2 norm of the residual by three orders of magnitude from its initial value. This was deemed sufficiently converged for comparison purposes. The 0 and 6.7 degree angle-of-attack cases were run without any problems. For the 14 degree angle-of-attack cases, the restart file from the 1,500 iteration 6.7 degree case was used to nudge the angle-of-attack up to 8 degrees, then 10, 12, and finally 14 degrees. Each successive increase was run 500 iterations.

ZEUS

An inviscid, finite volume, spatial marching flow solver was also used to predict surface pressures on the cone-cylinder configuration. The Zonal Euler Solver (ZEUS) code, developed by Wardlaw, et al,[14] was selected because of its efficiency and robustness. The ZEUS code is suitable for computations where the flowfield is entirely supersonic about the body; and any canards, wings, or fins are thin relative to the body diameter. The code applies a zonal strategy which divides the computational domain into one or more zones, each of which can be mapped separately. Zone edges are defined by the user to coincide with the body and bow shock surfaces.[15]

The calculation of a body's flowfield is initiated near the nose tip and marched aft in a planar fashion along the body axis to the base. The initial starting flowfield is generated by an external source. For the geometry presented in this paper, a conical starting solution was employed.

The ZEUS code was used to calculate flowfield pressures and aerodynamic coefficients for this cone-cylinder configuration at Mach 6.86 for angles-of-attack of 0, 6.7, and 14 degrees.

Pressures between the body surface and the bow shock were calculated at grid cell centers. Surface pressures were integrated to provide the aerodynamic normal force coefficient, and to determine the location of the center-of-pressure.

Since the cone-cylinder is axisymmetric with no fins, only a single computational zone was used. Due to symmetry, the zone was established between the leeward and windward axes around one half of the body.

A 36 x 18 grid was employed across this zone. There were 36 grid cells equally spaced between the leeward and windward body meridians, and 18 clustered grid cells between the body surface and the bow shock. These cells were clustered radially so that grid points were concentrated close to the body.

The marching step size along the body axis was automatically varied as a function of the geometry, flow conditions, and Courant (CFL) factor. A default value of 0.9 was used for the CFL factor in each calculation.

Results

The results to be presented in this section will be comparisons between the experimental and the calculated axial and circumferential surface pressure distributions. Additionally, the calculated normal force coefficient and the location of the center-of-pressure will be compared to the experimental values. Finally, pressure contours from EAGLE predictions will be shown.

It should be noted that there was a discrepancy identified in the experimental report's conclusions of the quality of the pressure data. A slight deviation of the pressure on the forepart of the conical nose for the experimental data is considered to be the result of documented small surface irregularities which were incurred in machining operations, and whose effect is accentuated at the tip where the imperfections become relatively large in comparison to the local radius.[16] This deviation accounts for irregularities in the experimental data on the nose.

Figure 3 presents a comparison of the experimental and calculated surface pressure distribution for the leeward symmetry plane at 0 degree angle-of-attack. The calculations compare favorably with the data. Note the EAGLE code overpredicts the pressure drop across the Prandtl-Meyer expansion at the nose-cylinder juncture more than ZEUS does. This is evident in all the EAGLE and ZEUS prediction comparisons to follow.

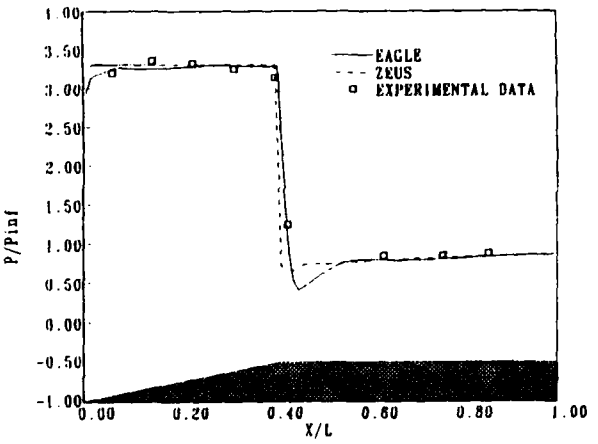

Figure 3. Experimental and numerical comparison, Mach 6.86, 0 degree angle-of-attack.

Figures 4, 5, and 6 show the surface pressure comparisons for the 6.7 degree angle-of-attack case at the leeward, 90 degree, and windward meridians. At the leeward meridian (Figure 4) the agreement with both EAGLE and ZEUS is poor. This is due to cross-flow effects in the experiment which generate a viscous layer on the leeward side. At the 90 degree (Figure 5) and windward (Figure 6) meridians, each code's surface pressure predictions show good agreement with the experimental data. Discrepancies at the nose tip in the experimental data may be attributed to model defects noted earlier.

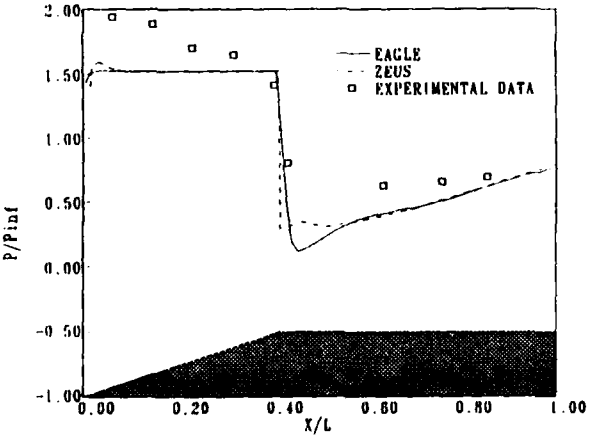

Figure 4. Experimental and numerical comparison, Mach 6.86, 6.7 degree angle-of-attack, leeward meridian.

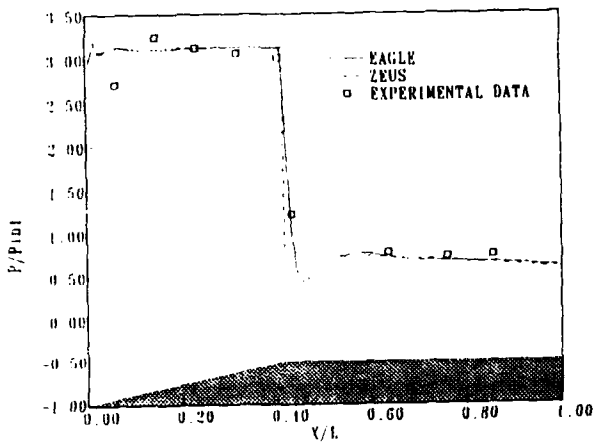

Figure 5. Experimental and numerical comparison, Mach 6.86, 6.7 degree angle-of-attack, 90 degree meridian.

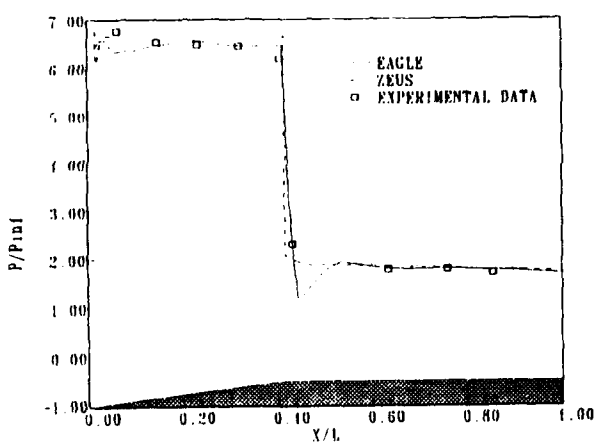

Figure 6. Experimental and numerical comparison, Mach 6.86, 6.7 degree angle-of-attack, windward meridian.

Figures 7 and 8 show circumferential surface pressure comparisons for the 6.7 degree angle-of-attack case at an axial location on the nose and on the cylindrical afterbody. The axial location on the nose (Figure 7) was at X/L = .231, and both codes show a slight deviation from experimental data at the leeward side (circumferential position of 0 degrees). Comparisons improve near the windward meridian. The axial location on the cylindrical afterbody (Figure 8) was at X/L = .758, and both EAGLE and ZEUS predictions deviate quite a bit from experimental data around the leeward meridian. Once again, predictions on the body toward the windward meridian improve and compare quite well. These two figures graphically display the cross-flow effects in the experiment which generated a viscous layer on the leeward side. As those effects became less pronounced circumferentially towards the windward meridian the codes predict surface pressure much better.

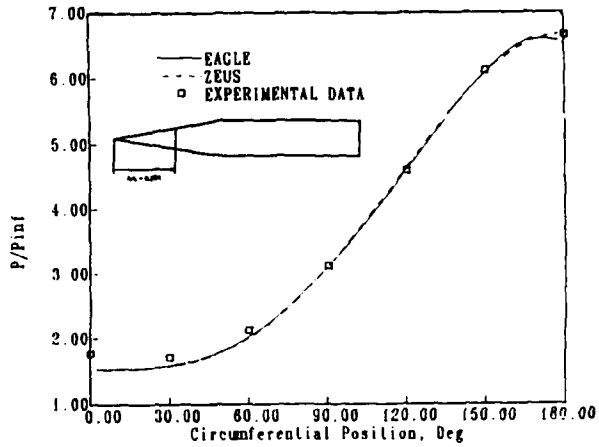

Figure 7. Experimental and numerical comparison, Mach 6.86, 6.7 degree angle-of-attack, X/L = 0.231.

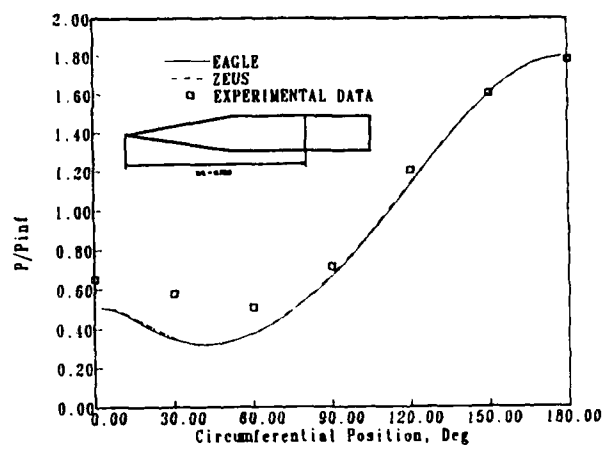

Figure 8. Experimental and numerical comparison, Mach 6.86, 6.7 degree angle-of-attack, X/L = 0.758.

Figures 9, 10, and 11 show the surface pressure comparisons for the 14 degree angle-of-attack case at the leeward, 90 degree, and windward meridians. At the leeward meridian (Figure 9), EAGLE and ZEUS predictions underestimate the surface pressures from the experiment. Experimental pressures are higher because the viscous layer has slowed down the flow on the leeward side, and the inviscid codes cannot catch this phenomenon. ZEUS predictions after the nose-cylinder juncture show a little ringing which is more than likely due to a step size that is too large for this region. At the 90 degree (Figure 10) and the windward (Figure

11) meridians, the codes show good agreement with experimental data. Both EAGLE and ZEUS experience oscillations of the flow solution at the nose tip.

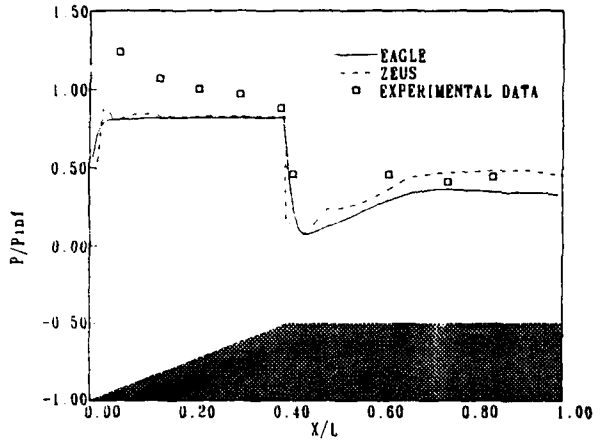

Figure 9. Experimental and numerical comparison, Mach 6.86, 14 degree angle-of-attack, leeward meridian.

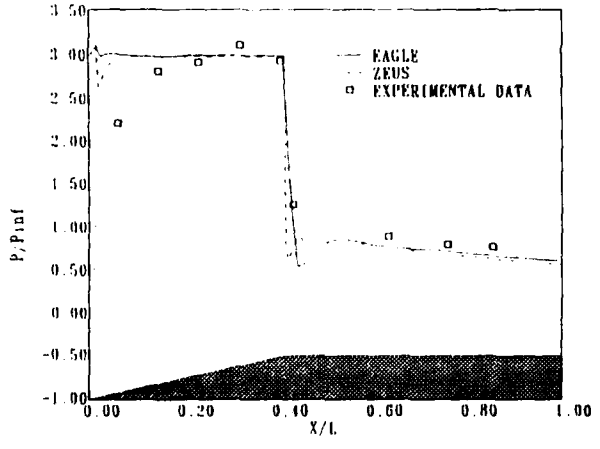

Figure 10. Experimental and numerical comparison, Mach 6.86, 14 degree angle-of-attack, 90 degree meridian.

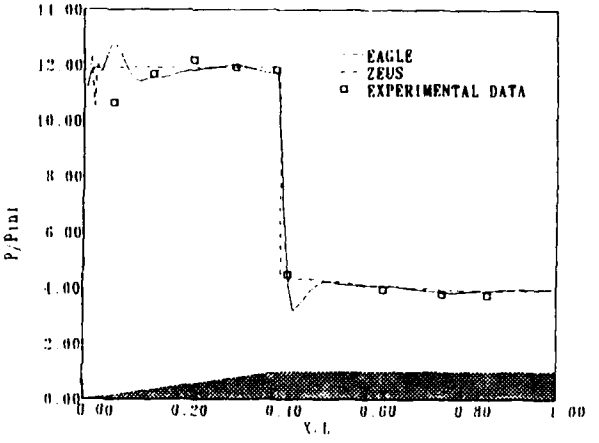

Figure 11. Experimental and numerical comparison, Mach 6.86, 14 degree angle-of-attack, windward meridian.

Figures 12 and 13 show the circumferential surface pressure comparisons for the 14 degree angle-of-attack case at an axial location on the nose and on the cylindrical afterbody. The axial location on the nose (Figure 12) was at X/L = .231, and both codes show a slight deviation on the leeward side just as the 6.7 degree angle-of-attack case did. The axial location on the cylindrical afterbody (Figure 13) was at X/L = .758, and the same type of correlation is shown. As stated for the previous case, the discrepancies on the leeward side are attributed to cross-flow effects in the experimental data which generate a viscous layer on the leeward side.

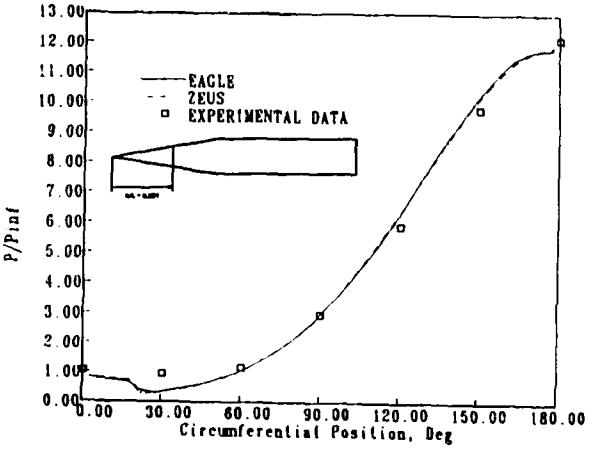

Figure 12. Experimental and numerical comparison, Mach 6.86, 14 degree angle-of-attack, X/L = 0.231.

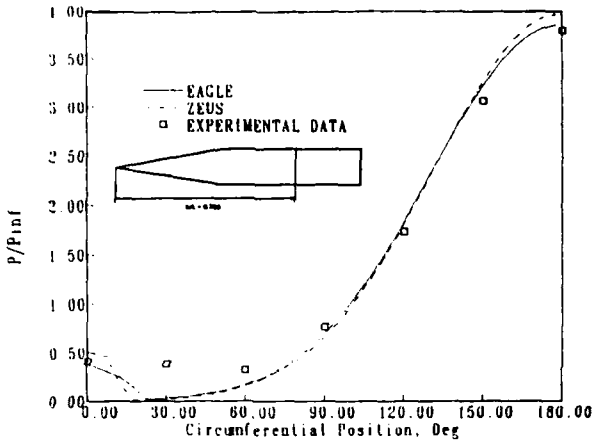

Figure 13. Experimental and numerical comparison, Mach 6.86, 14 degree angle-of-attack, X/L = 0.758.

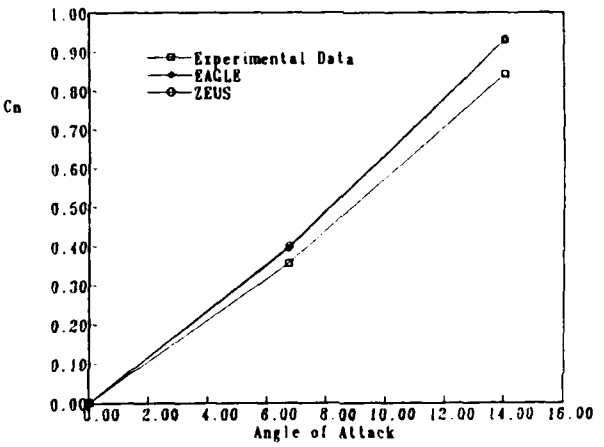

Figure 14. Normal force coefficient comparisons.

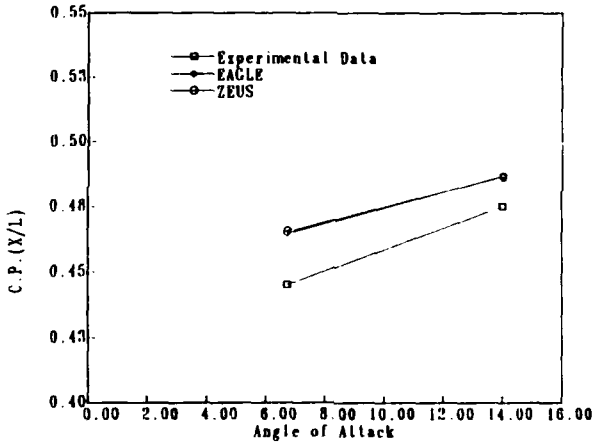

Figure 15. Center of pressure location comparisons.

Figures 14 and 15 present comparisons between the experimentally and numerically derived normal force coefficient, and the location from the nose tip of the center-of-pressure as a function of angle-of-attack. Both EAGLE and ZEUS predictions of normal force coefficient were larger than the normal force coefficient derived from the experiment. This is not surprising considering the surface pressure distribution comparisons on the leeward side of the configuration where viscous effects are more pronounced. Both codes consistently underpredicted the pressure distribution at and around this meridian, thereby making the normal force coefficient slightly greater than the coefficient determined in the experiment. Notice also that the codes successfully predicted the nonlinearity of the normal force coefficient curve. Figure 14 shows that both EAGLE and ZEUS predict the center-of-pressure location farther aft than the experimentally determined location, although the predicted values are within 5% of the experimental values. The accuracy of the calculated location of the center-of-pressure is a good indication of the accuracy of the calculated pressure distribution. Both EAGLE and ZEUS do a very good job calculating pressure distribution.

Figures 16, 17, and 18 are static pressure contour plots from EAGLE flowfield predictions for the 0, 6.7, and 14 degree angle-of-attack cases. The attached shock-wave angles from these contours were compared to NACA TR 1135 values for conical flow and showed excellent agreement. Prandtl-Meyer expansions at the nose-cylinder junctures are clearly visible. A denser overall computational grid or clustered grid lines in those regions of sharp flowfield gradients would yield even better resolution of these flow features.

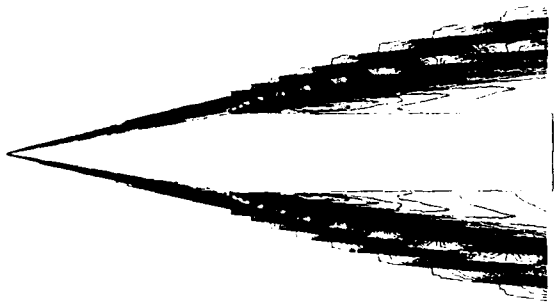

Figure 16. Pressure contour plots from EAGLE code, Mach 6.86, 0 degree angle-of-attack.

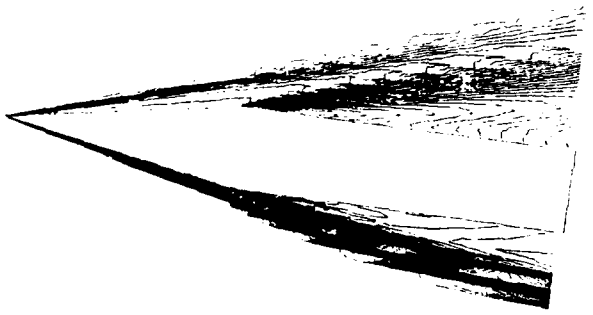

Figure 17. Pressure contour plots from EAGLE code, Mach 6.86, 6.7 degree angle-of-attack.

Figure 18. Pressure contour plots from EAGLE code, Mach 6.86, 14 degree angle-of-attack.

Conclusions

Hypersonic flowfield predictions have been computed for a cone-cylinder configuration using EAGLE code and ZEUS code at Mach 6.86 and 0, 6.7, and 14 degrees angle-of-attack. EAGLE code predictions of surface pressure distributions, normal force coefficient, and center-of-pressure location were very close to ZEUS predictions, and both codes compared favorably to the experimental data in those regions where viscous effects were minimal. These results represent a first step toward validating the EAGLE code in supersonic and hypersonic applications. This validation, coupled with EAGLE code's validation in the high subsonic and transonic flight regimes[8-12], will greatly expand its usefulness as a design tool.

References

1. McLellan, C. H., Williams, T. W., and Beckwith, I. E., "Investigation of the Flow Through a Single-Stage Two-Dimensional Nozzle in the Langley 11-Inch Hypersonic Tunnel," NACA TN 2223, 1950.

2. McLellan, C. H., Williams, T. W., and Bertram, M. H., "Investigation of a Two-Stage Nozzle in the Langley 11-Inch Hypersonic Tunnel," NACA TN 2171, 1950.

3. *Cooper, R. D. and Robinson, R. A.*, "An Investigation of the Aerodynamic Characteristics of a Series of Cone-Cylinder Configurations at a Mach Number of 6.86," NACA RM L51J09, 1951.

4. Lijewski, L. E., Cipolla, J. R., *Thompson*, J. F., and Gatlin, B., "Program EAGLE User's Manual, Volume I - Introduction and Grid Applications," AFATL-TR-88-117, Volume I, September 1988.

5. Thompson, J. F. and Gatlin, B., "Program EAGLE User's Manual, Volume II - Surface Generation Code," AFATL-TR-88-117, Volume II, September 1988.

6. Thompson, J. F. and Gatlin, B., "Program EAGLE User's Manual, Volume III - Grid Generation Code," AFATL-TR-88-117, Volume III, September 1988.

7. Mounts, J. S., Belk, D. M., and Whitfield, D. L., "Program EAGLE User's Manual, Volume IV - Multiblock Implicit, Steady-State Euler Code," AFATL-TR-88-117, Volume IV, September 1988.

8. Lijewski, L. E., "Transonic Flow Solutions on a Blunt, Finned Body of Revolutions Using the Euler Equations," AIAA-86-1082, 4th Fluid Mechanics, Plasma Dynamics and Lasers Conference, May 1986.

9. Cottrell, C. J., Martinez, A., and Chapman, G., "Study of Multi-Body Aerodynamic Interference at Transonic Mach Numbers," AIAA Journal, Volume 26, No. 5, pp. 553-560, May 1988.

10. Martinez, A., Chae, T. S., and Thompson, J. F., "Applications of Numerical Grid Generation to Advanced Weapon Airframe Configurations," AIAA-87-2294, Atmospheric Flight Mechanics Meet-ing, Monterey, CA, August 1987.

11. Cottrell, C. J. and Lijewski, L. E., "A Study of Finned, Multi-Body Aerodynamic Interference at Transonic Mach Numbers," AIAA-87-2480, 5th Applied Aerodynamics Conference, Monterey, CA, August 1987.

12. Lijewski, L. E., "Transonic Flow Solutions on a Blunt, Body-Wing-Canard Configuration Using an Explicit Euler Solver," AIAA-87-2273, 5th Applied Aerodynamics Conference, Monterey, CA, August 1987.

13. Ames Research Staff, "Equations, Tables, and Charts for Compressible Flow," NACA TR 1135, Ames Aeronautical Laboratory, Moffett Field, CA, 1953.

14. Wardlaw, A. B., Davis, S. F., and Priolo, F. J., "A Second Order Godunov's Method for Supersonic Tactical Missile Computations," Naval Surface Warfare Center, TR 86-506, December 1986.

15. Wardlaw, A. B. and Priolo, F. J., "Applying the ZEUS Code," Naval Surface Warfare Center, TR 86-508, December 1986.

16. Cooper, R. D. and Robinson, R. A., "An Investigation of the Aerodynamic Characteristics of a Series of Cone-Cylinder Configurations at at Mach Number of 6.86," NACA RM L51J09, 1951.

END

6-89

DTIC